HTML ABSTRACT + LINKS

A quasioptical transient electron spin resonance spectrometer operating at 120 and 240 GHz

J. van Tol and L.-C. Brunel
Center for Interdisciplinary Magnetic Resonance, National High Magnetic Field Laboratory at Florida State University, Tallahassee, Florida 32310

R. J. Wylde
Thomas Keating Ltd., Station Mills, Billingshurst, West Sussex, England and School of Physics and Astronomy, University of St. Andrews, North Haugh, St. Andrews, Fife, Scotland

(Received 23 November 2004; accepted 4 May 2005; published online 22 June 2005)

A new multifrequency quasioptical electron paramagnetic resonance (EPR) spectrometer is described. The superheterodyne design with Schottky diode mixer/detectors enables fast detection with subnanosecond time resolution. Optical access makes it suitable for transient EPR (TR-EPR) at 120 and 240 GHz. These high frequencies allow for an accurate determination of small g-tensor anisotropies as are encountered in excited triplet states of organic molecules like porphyrins and fullerenes. The measured concentration sensitivity for continuous-wave (cw) EPR at 240 GHz and at room temperature without cavity is 10^{13} spins/cm^3 (15 nM) for a 1 mT linewidth and a 1 Hz bandwidth. With a Fabry-Perot cavity and a sample volume of 30 nl, the sensitivity at 240 GHz corresponds to $\approx 3\times 10^9$ spins for a 1 mT linewidth. The spectrometer's performance is illustrated with applications of transient EPR of excited triplet states of organic molecules, as well as cw EPR of nitroxide reference systems and a thin film of a colossal magnetoresistance material. © *2005 American Institute of Physics.* [DOI: 10.1063/1.1942533]

I. INTRODUCTION

Electron paramagnetic resonance (EPR) at high frequencies plays an increasingly important role in a large variety of disciplines. Data obtained at a combination of EPR frequencies has illustrated the advantages of both high- and multifrequency EPR in a wide range of research topics from solid-state physics to biology.[1] Here we describe a multi- and high-frequency spectrometer designed for transient EPR experiments and which also is well suited for field-modulated continuous-wave (cw) EPR. While cw EPR in general studies ground-state paramagnetic systems, transient EPR or time-resolved EPR (TR-EPR) allows the study of short-lived paramagnetic species or excited paramagnetic states. These unstable species or metastable states are typically created by pulsed laser excitation.

Many of the high-frequency advantages for cw or pulsed EPR of ground-state systems or states apply equally to TR-EPR of transient systems or excited states. However, in particular, the increased Zeeman-splitting resolution and the increased time resolution warrant the availability of a high-frequency transient spectrometer. Generally, transient EPR spectra at conventional frequencies are entirely governed by the field-independent spin-spin and spin-orbit interactions while effects of g-tensor anisotropy are too small to be observed. At fields of 8.6 T (240 GHz) the effects of g anisotropy are enhanced by a factor of 25 with respect to X band and a g anisotropy of the order of 0.00005 can be easily measured. This is especially important for organic radicals and excited paramagnetic states of organic systems like those occurring in photosynthetic reaction centers.

High frequencies play a role also on the time parameter. First, the timescale of a cw EPR experiment shortens with increasing frequency in cases where the g anisotropy is appreciable. This has its influence on the measured spectra if the system under study involves molecular motion[2,3] or exchange coupling. Consequently, high field EPR is of great importance in the study of dynamics of molecules through its combination of higher g resolution and its sensitivity for shorter timescales. More relevant to transient EPR is the experimental aspect of an increased detection bandwidth. At conventional frequencies it is limited by the Q of the cavity ($\Delta\omega=\omega/Q$). High-frequency operation increases the detection bandwidth, which allows faster measurements, a feature particularly relevant for TR-EPR as well as for pulsed EPR. While for the latter the time resolution is limited by the power available for the micro/millimeter-wave pulses, there is no such restriction in TR-EPR. This is illustrated by the subnanosecond time resolution of the instrument described here.

The sensitivity in terms of the detectable number of spins in the sample improves with frequency. Under the assumption of identical experimental conditions, except for a scaling of resonator and sample size with the wavelength, and the condition of constant amplitude of the oscillating magnetic field (B_1) on the sample, Rinard *et al.* found a $\omega^{11/4}$ dependence,[4] in which ω is the EPR resonance frequency. Although in practice the experimental conditions will always be slightly different, especially at the very high frequencies that we are interested in here, this analysis appears in reasonable agreement with experimental observations.[5–7] Because the sample size is assumed to scale with ω^3, this im-

 © 2005 American Institute of Physics

Downloaded 09 Jan 2006 to 146.201.237.34. Redistribution subject to AIP license or copyright, see http://rsi.aip.org/rsi/copyright.jsp

plies that the concentration sensitivity is practically frequency independent, or actually very slightly deteriorates with increasing frequency($\omega^{-1/4}$).

In most TR-EPR experiments, the sensitivity improvement with increasing frequency is less favorable. In the majority of cases, the (optical) excitation induces a nonequilibrium population distribution of the sublevels of the paramagnetic system. This often is the principle reason that a signal can be observed at all. Though there can be a magnetic-field dependence of the population rates, whether induced by spin-orbit interaction mediated intersystem crossing mechanisms (SO-ISC) or by radical-pair mechanisms (RP-ISC), the order of magnitude of the population differences between the electron spin states does not depend on the frequency. In contrast, for ground-state systems in thermal equilibrium in the high-temperature limit ($\hbar\omega \gg kT$), the population difference is proportional to ω. Consequently, the sensitivity for spin-polarized systems that are encountered in TR-EPR is only proportional to $\omega^{7/4}$ instead of the $\omega^{11/4}$ for ground-state systems. This means that the concentration sensitivity for TR-EPR has a $\omega^{-5/4}$ frequency dependence. In the case of photoexcited states or photogenerated radicals the number of spins is always limited by the amount of photons absorbed, which in turn is limited by the sample-damage threshold.

While this sensitivity analysis[4] is valid for systems with a microwave cavity or resonator, if sufficient sample is available an arrangement without cavity is often preferable. Sample handling and alignment is greatly simplified, while similar or better concentration sensitivities can be achieved. Also it should be noted that phase noise tends to increase with frequency, and a cavityless arrangement is somewhat less sensitive to phase noise and microphonics. The typical sample size in the described system without cavity at both 120 and 240 GHz is similar to samples used at *X* band frequencies.

The quasioptical transient spectrometer is described below and some examples of applications of both cw EPR and TR-EPR are given.

II. EXPERIMENTAL SETUP

A. Multifrequency superheterodyne quasioptical bridge

The design of the spectrometer is based on the requirements of high time resolution and multifrequency operation, in order to make optimal use of the instrument for high-frequency TR-EPR. In our laboratory we also operate a multifrequency homodyne spectrometer that covers the frequency range from 190 to 400 GHz. The detector in that system is an InSb hot-electron bolometer, because its large frequency range of 50–1200 GHz makes it very suitable for a multifrequency setup. Their limited detection bandwidth of around 1 MHz,[8] however, makes InSb bolometers less suitable for time-resolved EPR. Therefore this transient spectrometer employs a (super)heterodyne detection scheme with high-frequency Schottky diode mixers. A detection bandwidth of the order of 1 GHz can be obtained, while the sensitivity is of the same order of magnitude or even better than that of bolometric detectors. The dedicated mixer/detectors and the neccessity of a second high-frequency source that serves as a local oscillator (LO) does limit the number of frequencies at which the spectrometer operates. The current standard operation frequencies are 120 and 240 GHz, while through interchange of the frequencies of the source and LO also 114 and 234 GHz can be used. An extension to 336 GHz is currently being implemented.

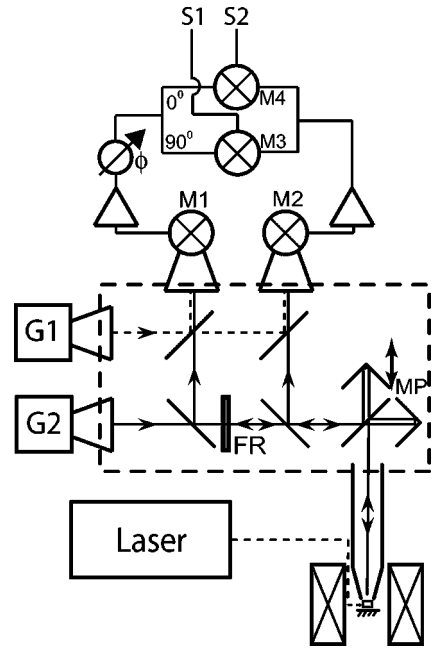

FIG. 1. Schematic experimental setup. G1: LO Gunn-diode, G2: Signal Gunn-diode, FR: Faraday-rotator, MP: Martin-Puplett interferometer, S1, S2: quadrature signal outputs, M1, M2: millimeter-wave single-ended Schottky mixers, M3, M4: 6 GHz balanced mixers.

In order to optimize sensitivity and minimize losses, a quasioptical design[9,10] is the most suitable. The multifrequency heterodyne bridge described here was adapted from the existing layouts for multifrequency homodyne quasioptical bridges[10] in cooperation with Thomas Keating Ltd. The latter company also fabricated the quasioptical elements.

The combination of circular corrugated waveguides, quasioptical techniques, and the direction of propagation of the radiation parallel to the magnetic field enables the use of "induction-mode" detection,[11] in a manner similar to that introduced by Smith *et al.*:[10,12] The magnetic dipolar absorption of only one of the two circular components of the incident linearly polarized radiation results in the generation of cross-polarized radiation. By detecting this cross-polarized component a reduction of 20–35 dB of the background is achieved, resulting in significantly improved sensitivity.

The schematics of the setup are shown in Fig. 1. The source millimeter waves are generated by a phase-locked 120 GHz Gunn diode (G2), which for operation at 240 GHz is fitted with a doubler (Radiometer Physics GmbH). Maximum powers are 40 mW at 120 GHz and 9 mW at 240 GHz. With minimal loss (0.3 dB) a corrugated horn transforms the TE_{01} mode in the single-moded waveguide into an HE_{11} mode in the circular guide and allows this to gently expand to an overmoded aperture with zero phase curvature. The

Downloaded 09 Jan 2006 to 146.201.237.34. Redistribution subject to AIP license or copyright, see http://rsi.aip.org/rsi/copyright.jsp

beam that propagates from this aperture is broadly Gaussian in nature.[13] From the horn the radiation enters the quasioptical millimeter-wave bridge (dotted region in Fig 1), where it passes through a variable attenuator (0–30 dB) and a circulator, consisting of a 45° Faraday rotator (a ferrite plate with antireflection coatings) in between a pair of wire-grid polarizers. The purpose of this circulator is to act as an isolator, thereby damping down standing waves, as well as to direct the copolar signal to the reference detector. The last element of the bridge, before the beam is fed into the oversized corrugated waveguide that leads the radiation to the sample, is a Martin-Puplett interferometer[14] which serves as a polarization converter. The inner diameter of the corrugated waveguide of the sample probe and all the source and detector corrugated horns is about 18 mm at 240 GHz and 22 mm at 120 GHz. The quasioptical bridge is completely frequency independent in the range of 120–500 GHz, except for the Faraday rotator. The antireflection coatings were optimized for 240 GHz. The performance at 120 GHz of the quasioptical circulator, however, is good enough for its use at that frequency without exchanging the Faraday rotator. The slightly higher losses are generally not an issue as more than enough power is available at that frequency.

The returning radiation is split into two components by a wire grid polarizer. The copolarized beam goes back to the circulator and from there is led to the reference Schottky diode mixer (M1), while the cross-polarized beam is led to the signal Schottky diode mixer (M2). To both of these beams a signal from a second Gunn oscillator is added within the quasioptical bridge. This second diode operates 6 GHz below the source frequency (114 GHz, and in combination with a doubler, at 234 GHz), and provides the local oscillator signal for the two Schottky diode mixers. Both the 120 GHz mixers (Farran Technology Inc.) and the 240 GHz mixers (Radiometer Physics GmbH) are single-ended (signal and LO enter through the same port) fundamental mixers. They use a local oscillator level of around 500 μW and have a typical single side band (SSB) conversion loss of 12 dB. This corresponds to a noise power at the millimeter-wave frequency of approximately 3×10^{-19} W/Hz. Both of the millimeter-wave mixers as well as both the Gunn/multiplier combinations are equipped with corrugated horns.

Without sample, the total estimated losses from source to reference detector with a metallic mirror at the sample position is of the order of 5–6 dB, a large part of which is due to the insertion loss of the Faraday-rotator (2–3 dB per pass). With sample the losses in general are higher, and depend on the sample absorption as well as its size and shape. However, at powers between 0 and 13 dB attenuation (9 mW–500 μW at 240 GHz), source noise tends to be larger than detector noise, and losses in the sample do not influence the signal-to-noise ratio if these losses are less than 10 dB.

The resulting 6 GHz intermediate frequency (IF) signals from the two mixers are amplified by low-noise amplifiers (Miteq), pass through variable attenuators, and are mixed down to dc by 6 GHz mixers in a quadrature detection scheme (Fig. 1) . A 6 GHz phase shifter in the reference channel allows for phase tuning. The quadrature detection is very useful especially in the absence of a cavity or resonator,

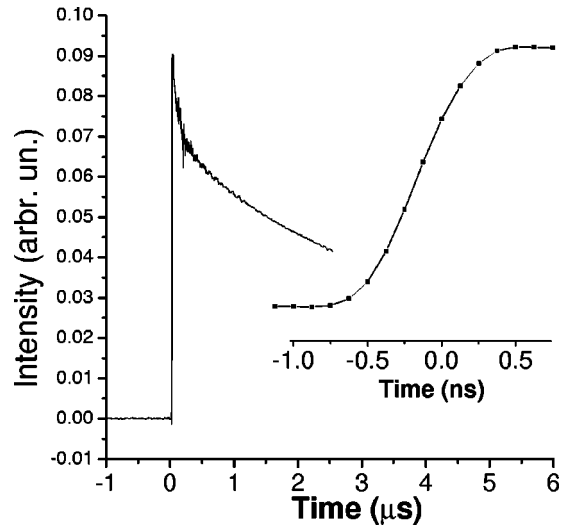

FIG. 2. Response of the reflection of a Si wafer to a 110 ps laser pulse at 532 nm. The structure at a few hundred ns is artifact due to electrical pickup from the Q switch of the laser.

as there is no good *a priori* experimental criterion to optimize the phase in order to obtain pure absorption. Almost always a mixture of absorption and dispersion is measured. The availability of two signals that are 90° out of phase allows for *a posteriori* phase correction of the data, or serves to decrease the error margins of the parameters by fitting both spectra with a simulation/fitting program that allows for a mixture of real and imaginary parts of the susceptibility.

The signals from the two 6 GHz mixers (M3 and M4 in Fig. 1) are led to a pair of lock-in amplifiers (Stanford Research systems 830) for field-modulated cw EPR or to a digital oscilloscope (HP Infinium 54825A) in the case of transient EPR. While the superheterodyne detection scheme as shown in Fig. 1 may appear quite conventional, several aspects of this spectrometer are unusual, and are discussed in more detail in the following paragraphs.

The relatively high intermediate frequency was chosen to obtain a large detection bandwidth of around 1 GHz. The limitation for the time resolution in an EPR experiment is mostly related to the bandwidth of the cavity given by $\omega/2\pi Q$ and usually is of the order of 10–100 MHz. In this case, when no high Q cavity is employed, the time resolution is limited by the detection electronics. The bandwidth was tested via the excitation of a Si wafer with a 110 ps laser pulse at 532 nm. The resulting signal is shown in Fig. 2. The measured initial response from 95% to 5% transmission occurs within 600 ps, which characterizes the time resolution of the detection system. The opening of the switch corresponding to the decay from the conduction band takes place over a much longer time scale.

The Martin-Puplett interferometer serves as a polarization converter and is located between the corrugated waveguide of the probe and the wire grid that separates the co- and cross-polarized signals. It essentially splits the incoming linearly polarized beam into two $\pm45^\circ$ polarized beams and recombines them with a variable phase shift.[14] The linearly polarized incoming beam can thus be converted into left- or right-hand circular polarization or into the perpendicular lin-

Downloaded 09 Jan 2006 to 146.201.237.34. Redistribution subject to AIP license or copyright, see http://rsi.aip.org/rsi/copyright.jsp

ear polarization. In the employed geometry, the millimeter waves travel along the static magnetic field direction and, for a typical $S=1/2$ system, the use of the appropriate circular polarization results in the strongest absorption. However, it does not result in optimal sensitivity because it does not allow for the background reduction that is achieved with linear polarization and induction-mode detection. As opposed to a fixed linear polarizer, the Martin-Puplett allows for some optimization (i.e., minimization) of the detected cross-polarized polarization. The latter is generated by deviations from cylindrical symmetry induced by the sample and/or imperfections in the waveguide. For samples or sample configurations in which only one of the linear polarization components is absorbed, this standard induction-mode detection cannot be employed. But the Martin-Puplett allows the use of an alternative induction-mode detection using the circular polarizations: With incident right (left) circular polarization, a linearly polarized absorption induces intensity in the other circular component. This can, for example, be favorably employed to measure thin films with the dc magnetic field in the plane of the film, and the millimeter-wave propagation direction perpendicular to the plane of the film and the dc magnetic field.

While the cross-polarized component provides the signal, the reference signal is generated from the copolarized component. This particular scheme was implemented to minimize both the phase noise as well as the phase drift. Phase noise at these high frequencies is a concern. For these multiplied sources the phase noise, expressed in units of dB, increases with $20 \log n$ in which n represents the multiplication factor with respect to the base frequency. In our case both Gunns are phase locked to two 4.5–4.8 GHz frequency synthesizers, and $n=25$ for 120 GHz and $n=50$ for 240 GHz, resulting in a phase noise degradation of 28 and 34 dB, respectively. Another concern is phase stability and/or phase drift. The short wavelength makes the system very sensitive to temperature changes. Upon cooling from room temperature to 4 K the distance traveled by the millimeter waves from source to detector changes by approximately 5 mm, corresponding to four wavelengths at 240 GHz. The generation of the reference signal as shown in Fig. 1 not only compensates part of the phase noise of the millimeter-wave sources, but also eliminates phase drift induced by path length changes, by ensuring that both 6 GHz source and reference signals are generated by the same millimeter-wave sources and by beams having traveled exactly the same distance, independent of the actual path length.

B. Sample configuration

The sample is mounted on the sample probe inside a variable temperature dynamic flow cryostat. The millimeter radiation propagates to the sample via an oversized circular corrugated waveguide of about 1.2 m length and 18 mm (22 mm at 120 GHz) diameter. A linear corrugated taper/horn at the bottom of the waveguide reduces the diameter to about 5 mm at 240 GHz and 6.4 mm at 120 GHz. At the end of this taper a variety of sample holders can be mounted dedicated to the type of measurement and the sample characteristics (see Fig. 3). The maximum active sample volume is of the order of 100 mm^3, and accommodates sample shapes ranging from thin films to sealed X-band EPR tubes. The modulation coil for cw EPR is integrated in the sample holders.

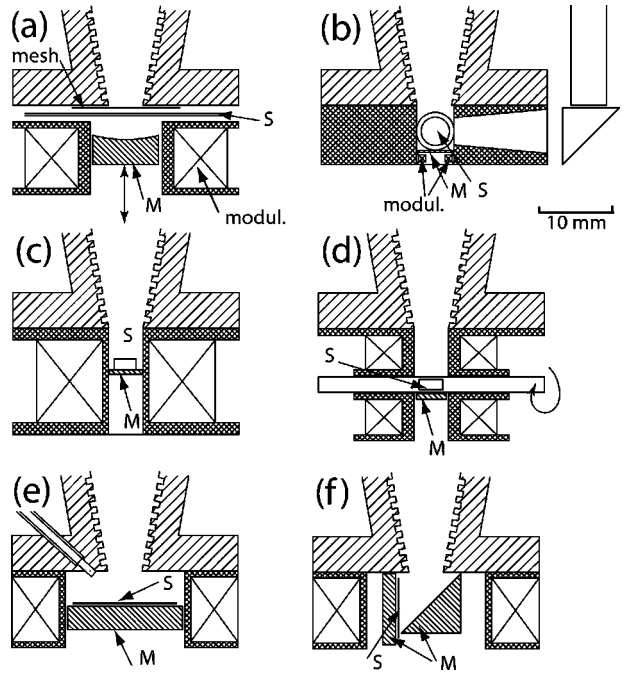

FIG. 3. Sample holder configurations. (a) Fabry-Perot cavity. (b) 5 mm o.d. quartz tube with optical excitation for TR-EPR. Excitation light arrives from the side from a quartz light guide via a right-angle prism. (c) cw EPR of solid or powdered sample. For powders a teflon or rexolite holder is used. (d) Single crystal with single axis rotation; (e) Thin-film $\perp B$ with optional optical excitation through a multimode 600 μm optical fiber. (f) Thin-film $\parallel B$. S labels the sample position, while M designates the position of the curved (a) or flat [(b)-(f)] mirrors. The position of the field modulation coils is given by the areas with a diagonal cross.

A typical configuration for transient EPR is shown in Fig. 3(b). The sample is contained in an aluminum holder, which is open on the top for the millimeter waves and on one side for optical access. A small modulation coil below the sample allows for a g marker to be included during the measurement. Optical excitation of the samples can be achieved by either a 6 ns Q-switched Nd-YAG laser (PowerLite 9010, Continuum, Santa Clara, CA), or a custom mode-locked Nd-YAG laser (Continuum PY-90C) delivering 110 ps pulses and that is used in combination with an optical parametric oscillator. The light is delivered to the sample with a 4 mm fused silica lightguide and a right-angle prism [see Fig 3(b)], or by one or more relatively thick (600 μm) multimode fibers [see Fig 3(e)].

For nonlossy samples at these frequencies there is no great advantage in the use of a cavity or resonator, provided a sufficient quantity is available. If the latter is not the case, however, and for lossy samples like aqueous solutions, the use of a resonator becomes a necessity. This spectrometer uses a semi-confocal Fabry-Perot resonator, with a Q of the order of 4000 with about 8 half-wavelength distance ($\approx$5 mm at 240 GHz) between the mirrors. The coupling mirror is either a gold mesh on a thin quartz substrate or a free standing copper mesh. A gold-coated fused silica plano-concave lens serves as the spherical mirror, and a distance adjustment via a differential screw mechanism allows for the

Downloaded 09 Jan 2006 to 146.201.237.34. Redistribution subject to AIP license or copyright, see http://rsi.aip.org/rsi/copyright.jsp

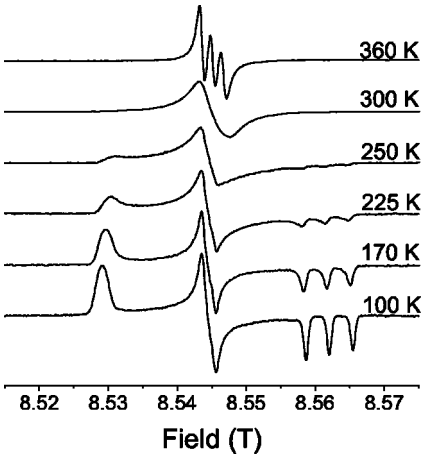

FIG. 4. 240 GHz spectra of TEMPO (0.009 wt. %, 650 μM) dissolved in polystyrene containing 7 wt. % toluene as a function of temperature. Incident power on sample 120 μW (−16 dB). The intensities are corrected for the employed modulation amplitude, which was 0.15 mT for $T<300$ K and 0.4 mT for $T\geqslant 300$ K. Time constant 0.3 ms. Single scans at 0.1 and 0.2 mT/s.

tuning of the cavity. The sample is placed in a quartz capillary tubing (0.2 mm i.d. for 120 GHz, 0.1 mm i.d. at 240 GHz). Other than the fact that the same resonator can be used at different frequencies, a principle reason for choosing a Fabry-Perot resonator over a cylindrical cavity is that it allows the use of inductive-mode detection, in a similar way as in an arrangement without a resonator. Although in practice the isolation between the copolarized and cross-polarized components in the cavity dip is somewhat reduced, it still improves the signal-to-noise ratio. As currently no mechanism is employed for coupling optimization, the coupling typically is of the order of 90%. The same resonator is used at both 120 and 240 GHz. Only the mesh is changed depending on the frequency.

For cw EPR of powders, frozen solutions, ceramics, etc., a sample configuration as illustrated in Fig. 3(c) is used, in general with a Teflon sample cup. For single crystals a single-axis rotator can be employed, as illustrated in Fig. 3(d). For thin films with larger surfaces typically the sample holders (e) and (f) are used for measurements with the plane of the film perpendicular and parallel to the magnetic field, respectively.

III. RESULTS AND DISCUSSION

A. Continuous-wave EPR

The sensitivity in an EPR experiment is usually expressed in terms of the number of detectable spins for a resonance line with a width of 1 G (0.1 mT) or 1 mT for a 1 Hz bandwidth, and typically is of the order of 10^{11} spins/mT (10^{10} spins/G) at *X*-band frequencies. In order to evaluate the sensitivity for this high-frequency spectrometer, typical spectra for a nitroxide radical are shown in Fig. 4. The incident power on the sample was kept constant for all temperatures, but it should be noted that the integrated intensity of the high temperature spectra are weaker (up to a factor of 4) than can be expected by the change in temperature alone. This is probably due to increased losses in the sample at high temperatures. This reference sample was made by dissolving 2,2,6,6-tetramethyl-1-piperidinyloxy (TEMPO) into a solution of polystyrene in toluene and subsequently drying the sample in air until it contained about 7 wt. % of toluene. The TEMPO concentration corresponds to 0.009 wt. % or 650 μM. Figure 3(c) shows the sample geometry, with a total volume of 80 μl, which corresponds to a total number of spins in the sample of 3×10^{16}(50 nmol).

The presence of toluene allows for a considerable motion of the nitroxide which gives rise to the strong temperature dependence of the measured spectra. The motional correlation time varies from about 100 ps at 360 K to longer than 1 μs at 100 K. In order to avoid saturation at the lowest temperatures, the microwave power was attenuated by 16 dB from the maximum power and is about 100 μW at the sample. This corresponds to a maximum B_1 field of the order 1×10^{-6} T. The intensities shown in Fig. 4 are corrected for the modulation amplitude, which was 0.15 mT for $T<300$ K and 0.4 mT for $T\geqslant 300$ K. The spectra are single scans recorded with a time constant of 300 ms. The spectral shape obviously has an influence on the sensitivity that can be obtained. At low temperatures the total width of the spectrum at 240 GHz for these nitroxides is about 40 mT, but for optimum resolution the modulation amplitude has to be limited to 0.15 mT. On the other hand, the intensities of the derivative spectrum are determined by the linewidths at the canonical directions rather than the total linewidth. However, the spectrum at 300 K can be roughly approximated by a Lorentzian line with a full width at half-height (FWHH) of 6.8 mT, which is more convenient for the sensitivity estimate. If we define the signal-to-noise ratio (SNR) as the $V_{p-p}^{\text{signal}}/2*V_{RMS}^{\text{noise}}$ we obtain SNR$\approx$1500. With extrapolation to a modulation corresponding to 1/3 of the linewidth instead of the 0.4 mT we obtain a sensitivity at 300 K of the order of 7×10^{11} spins for a 1 mT linewidth and a 1 Hz bandwidth. This corresponds to a concentration sensitivity of about 15 nM/mT or 10^{13} spins/(mT cm^3). The convention used here to define the 1 Hz bandwidth is to renormalize the measured S/N ratio to a time constant of $0.16(1/2\pi)$s. All spectra here are recorded with a 0.3 s time constant, and for the calculation of the sensitivity the obtained S/N ratio is multiplied by $\sqrt{0.16/0.3}$. The sample volume is quite comparable to that at *X* band, and we can conclude that the concentration sensitivity in this setup without cavity at 240 GHz is comparable to that at *X* band within an order of magnitude. From the expected frequency dependence ($\omega^{-1/4}$) of the concentration sensitivity in case of a similar cavity (assuming equal B_1 fields),[4] it is clear that in terms of concentration sensitivity the use of a cavity will not provide large gains.

In case of small samples or in the case of lossy samples like aqueous solutions, the use of a cavity of course *is* warranted. For that purpose the Fabry-Perot cavity as shown in Fig. 3(a) can be used. Typical signals obtained for a 100 μM aqueous solution of 4-hydroxy-2,2,6,6-tetra-methyl-piperidinyl-oxy (TEMPOL) are shown in Fig. 5. The sample is mounted in a quartz capillary with an inner diameter of 0.2 and 0.1 mm for 120 and 240 GHz, respectively. The corresponding active sample volume is 120 nl at 120 GHz and 30 nl at 240 GHz, thus containing 12 and 3 pmol of nitroxide

Downloaded 09 Jan 2006 to 146.201.237.34. Redistribution subject to AIP license or copyright, see http://rsi.aip.org/rsi/copyright.jsp

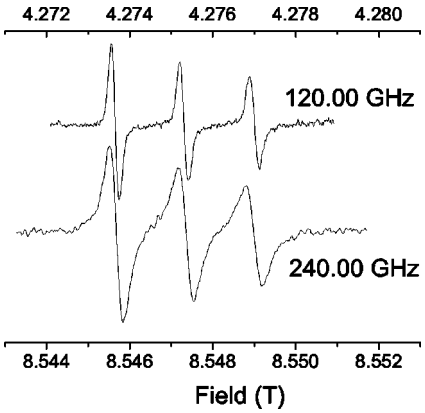

FIG. 5. Spectra of 100 μM solution of 4-hydroxy-TEMPO in H_2O at 293 K at 120 GHz and 240 GHz, using a Fabry-Perot cavity. Single scans at 0.05 mT/s with 0.3 s time constant.

spins, respectively. The spectra shown in Fig. 5 correspond to single scans at 0.025 mT/s (120 GHz) and 0.05 mT/s (240 GHz) and a time constant of 0.3 s. The obtained sensitivity is of the order of 9×10^9 and 3×10^9 spins for a 1 mT linewidth at 120 and 240 GHz, respectively, for these aqueous samples. This corresponds to a concentration sensitivity of around 140 nM/mT (or 10^{14} spins per cm^3 for a 1 mT linewidth). For nonlossy solid samples the absolute sensitivity is of the order of 2×10^9 spins/mT(2×10^8spins/G) at 240 GHz at room temperature.

B. Transient EPR of excited triplet states

One of the typical systems in which transient EPR can be observed is the porphyrin ring and its many derivatives, which play an important role in many biological systems, like the photosynthetic reaction centers. The zero-field splitting generally is of the order of 1 GHz, while the *g* factor at low frequencies is unresolved. At the very high frequencies used in the instrument described here, however, the *g* anisotropy is clearly resolved and corresponds to shifts that are of the order of 9 mT (250 MHz). This not only enables an accurate measurement of the *g* anisotropy of the excited triplet state, but also can provide information about the relative orientation of the canonical directions of the zero-field splitting tensor with respect to those of the *g* tensor. In Fig. 6 the transient EPR spectrum of tetra-phenyl porphyrin (TPP) dissolved in polystyrene at 240.00 GHz is shown. The obvious asymmetry in the spectrum is due to the *g* anisotropy. For a more complete description see Ref. 15. While the high-frequency TR-EPR spectra for TPP can be accurately fitted by assuming coaxial ZFS and *g* tensors, for the excited triplet state of the primary donor of the photosynthetic reaction center of Rhodobacter Sphaeroides R26, the resolution at 240 GHz proved sufficient to assign a relative rotation of ZFS and Zeeman splitting tensors.[16]

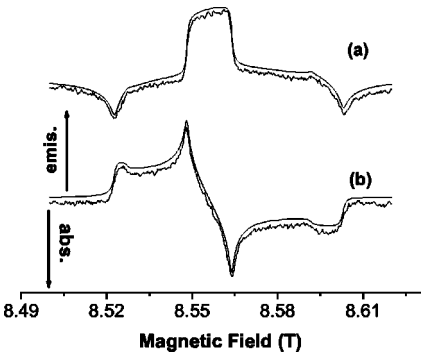

FIG. 6. Real (a) and imaginary (b) component of the susceptibility at 240 GHz of the lowest triplet excited state of tetra-phenyl porphyrin in polystyrene at 170 K. Drawn lines represent fits to the Hamiltonian $\mathcal{H}=D(S_z^2-\vec{S}^2/3)+E(S_x^2-S_y^2)+\vec{S}\cdot\vec{\vec{g}}\cdot\vec{B}$ with a *g* tensor that is diagonal in the ZFS axis system.[15]

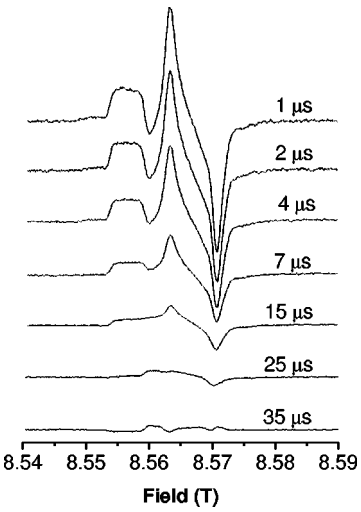

FIG. 7. Excited triplet state transient EPR spectrum of the trans-4 fullerene bisadduct $C_{60}(C-(COOEt)_2)_2$ as a function of the time after the laser pulse.

The typical sample size used in these experiments is very similar to that at *X* band. In most cases the sample is contained in a short 4 mm outer diameter (o.d.) quartz tube that is placed horizontally in the sample holder, and corresponds to an active sample volume of the order of 30 μl. For field calibration, a reference sample is placed on the mirror under the sample tube. A small modulation coil under the mirror [Fig. 3(b)] enables the detection of the cw EPR signal of the reference sample simultaneously with the directly detected transient signal.

Figure 7 shows an example of a fullerene excited triplet state. The spectrum of the *trans*-4 bis $(-C((CH_2)COOH)_2$ fullerene biadduct in PMMA as a function of the time after the laser pulse illustrates the anisotropy of the relaxation at 100 K. A description of the obtained results in a variety of fullerene adducts is given elsewhere.[17–19] In this example the power incident on the sample is about 50 μW. The B_1 field at this power in the cavityless configuration is of the order of 1 μT. While this precludes the observation of transient nutation effects, it enables the determination of relatively long relaxation and/or triplet lifetimes.

C. Thin films

Magnetic resonance at high fields is of particular interest for thin films of magnetic materials. Bulk measurements of magnetization and susceptibility are not straightforward because the thickness of the film needs to be precisely known, while only average values of magnetization can be measured.

Downloaded 09 Jan 2006 to 146.201.237.34. Redistribution subject to AIP license or copyright, see http://rsi.aip.org/rsi/copyright.jsp

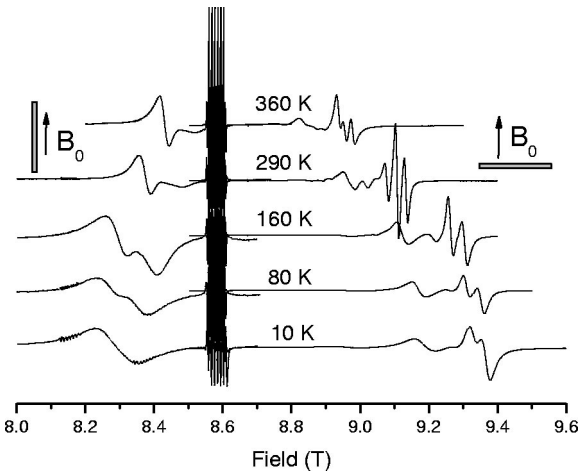

FIG. 8. EPR (FMR) spectra of a thin film of $La_{0.67}Sr_{0.33}MnO_3$ film on MgO at 240.00 GHz as a function of temperature. The sharp signals at 8.6 T are due to Mn^{2+} impurities in the substrate. Signals on the low-field side correspond to spectra taken with B_0 in the plane of the film, while signals on the right show the spectra with B_0 perpendicular to the plane of the film.

Also paramagnetic impurities in the substrate material can give a significant contribution. The setup without resonator is well suited for the study of these kind of systems, as it can accommodate samples with a relatively large surface area, while essentially the same setup and sample can be used at different frequencies and fields.

An example is shown in Fig. 8 for a 500 nm film of $La_{0.67}Sr_{0.33}MnO_3$ on a MgO substrate, grown by chemical vapor deposition. The intense sharp features are due to Mn^{2+} impurities in the MgO substrate, the position of which is independent of temperature and sample orientation. The broader features are from the manganite film: those on the high-field side are measured with B_0 perpendicular to the plane of the film [Fig. 3(e)], while those on the low-field side are measured with B_0 in the plane of the film [Fig. 3(f)].

The shifts of the resonance lines in these ferromagnetic films are due to the temperature dependence of the sample magnetization. With the film perpendicular to the magnetic field, the demagnetization factor for a perfect thin film is 1.0, while it is −0.5 for the magnetic field in the plane of the film. The structure in this particular case indicates that the film is not isotropic, but that different zones can be distinguished with different magnetization and/or the existence of microstructures. The latter has been indicated by transmission electron microscopy.[20] The zone with the largest shift corresponds to a saturation volume magnetization of 5.78×10^5 A/m. With the measured g value of 1.991 this corresponds to an effective magnetization of 3.64 Bohr magneton per manganese atom, which is very close to the expected value of 3.67 μ_B.

The sample configuration is as shown in Fig. 3(e) for the direction of the magnetic field perpendicular to the film surface. For the configuration with the magnetic field in the plane of the film, the best signal-to-noise was achieved with a 45° mirror as shown in Fig. 3(f) in order to keep the millimeter waves perpendicular to the plane of the film. Because in that case only the component of B_1 perpendicular to the static magnetic field B_0 contributes to the magnetic dipole transition, the usual inductive mode detection[10] cannot be used. However, the Martin-Puplett interferometer enables the application of an equivalent detection scheme. In the "normal" induction-mode detection, linearly polarized millimeter-wave radiation is incident on the sample and the cross-polarized radiation is detected that is generated through the circularly polarized magnetic dipole transition probability for (sub)millimeter waves propagating along the field axis. Equivalently, if the transition is linearly polarized, one can use incident circularly polarized millimeter waves. The linearly polarized transition then induces intensity in the other circular component, which we can use as our signal channel. The roles of the two single-ended Schottky mixers (M1 and M2 in Fig. 1) are interchanged because the reflected circular radiation after passing the Martin-Puplett interferometer will be cross-polarized with respect to the linear polarized beam that is incident on the Martin-Puplett. Due to the symmetry of the experimental setup, this does not pose a problem. The only change necessary for this "inverted induction-mode detection," other than the setting of the Martin-Puplett interferometer, is the interchange of the RF and LO connections of the 4-8 GHz mixers (M3 and M4 in Fig. 1). The difference in signal intensity ("isolation") that can be achieved is of the same order as for the linear polarization, i.e., 20-35 dB. The signal-to-noise is of the same order of magnitude as obtained with the usual induction-mode detection.

The spectrometer described here is available for external users for cw EPR or transient EPR experiments at 120 and 240 GHz as a part of the National High Magnetic Field Laboratory facility (see http://users.magnet.fsu.edu).

ACKNOWLEDGMENTS

This work was supported by the National Science Foundation under grant No. CHE-9601731. The authors would like to thank A. L. Maniero, M. Bortolus, and M. Prato for the fullerene bisadduct sample, and K. H. Dahmen and N. Mateeva for the LSMO thin film.

[1] *Very High Frequency (VHF) ESR/EPR*, edited by O. Grinberg and L. J. Berliner, Vol. 22 of Biological Magnetic Resonance (Kluwer Academic/Plenum, New York, 2004).
[2] Z. C. Liang and J. H. Freed, J. Phys. Chem. B **101**, 6384 (1999).
[3] K. A. Earle and A. I. Smirnov, *Very High Frequency (VHF) ESR/EPR*, Vol. 22 of Biological Magnetic Resonance (Kluwer Academic/Plenum Publishers, New York, 2004), Chap. 4, p. 95144.
[4] G. A. Rinard, R. W. Quine, J. R. Harbridge, R. T. Song, G. R. Eaton, and S. S. Eaton, J. Magn. Reson. **140**, 218 (1999).
[5] D. Schmalbein, G. G. Maresch, A. Kamlowski, and P. Hofer, Appl. Magn. Reson. **16**, 185 (1999).
[6] R. T. Weber, J. A. J. M. Disselhorst, L. J. Prevo, J. Schmidt, and W. T. Wenckebach, J. Magn. Reson. (1969-1992) **81**, 129 (1989).
[7] O. Burghaus, M. Rohrer, T. Gotzinger, M. Plato, and K. Mobius, Meas. Sci. Technol. **3**, 765 (1992).
[8] A. K. Hassan, L. A. Pardi, J. Krzystek, A. Sienkiewicz, P. Goy, M. Rohrer, and L. C. Brunel, J. Magn. Reson. **142**, 300 (2000).
[9] K. A. Earle, D. S. Tipikin, and J. H. Freed, Rev. Sci. Instrum. **67**, 2502 (1996).
[10] G. M. Smith, J. C. G. Lesurf, R. H. Mitchell, and P. C. Riedi, Rev. Sci. Instrum. **69**, 3924 (1998).
[11] A. M. Portis and D. T. Teaney, J. Appl. Phys. **29**, 1692 (1958).
[12] G. M. Smith and P. C. Riedi, *Progress in High Field EPR*, Vol. 17 of the Royal Society of Chemistry Specialists Periodical Reports (RSC, Cambridge, UK, 2000), p. 164.

Downloaded 09 Jan 2006 to 146.201.237.34. Redistribution subject to AIP license or copyright, see http://rsi.aip.org/rsi/copyright.jsp

[13] R. J. Wylde, IEE Proc., Part H: Microwaves, Opt. Antennas **131**, 258 (1984).
[14] D. H. Martin and E. Puplett, Infrared Phys. **10**, 105 (1970).
[15] J. van Tol, L. C. Brunel, and A. Angerhofer, Appl. Magn. Reson. **21**, 335 (2001).
[16] R. H. Zeng, J. van Tol, A. Deal, H. A. Frank, and D. E. Budil, J. Phys. Chem. B **107**, 4624 (2003).
[17] L. Pasimeni, M. Ruzzi, M. Prato, T. Da Ros, G. Barbarella, and M. Zambianchi, Chem. Phys. **263**, 83 (2001).
[18] T. Da Ros, M. Prato, D. M. Guldi, M. Ruzzi, and L. Pasimeni, Chem.-Eur. J. **157**, 816 (2001).
[19] M. Bortolus, M. Prato, J. van Tol, and A. L. Maniero, Chem. Phys. Lett. **398**, 228 (2004).
[20] Y. Xin, K. Han, N. Mateeva, H. Garmestani, P. Kalu, and K. H. Dahmen, J. Mater. Res. **16**, 3073 (2001).

Downloaded 09 Jan 2006 to 146.201.237.34. Redistribution subject to AIP license or copyright, see http://rsi.aip.org/rsi/copyright.jsp